Journal of Chromatography A 1730 (2024) 465102

Contents lists available at ScienceDirect

Journal of Chromatography A

journal homepage: www.elsevier.com/locate/chroma

Antibody-ligand interactions on a high-capacity staphylococcal protein A resin

Rupert Tscheliessnig [a,b,f,g], Goncalo L. Silva [a], Jacek Plewka [b,c], Leo A. Jakob [a,b], Helga Lichtenegger [c], Alois Jungbauer [a,b,*], Ana C. Dias-Cabral [d,e]

[a] Austrian Centre of Industrial Biotechnology, Muthgasse 18, Vienna 1190, Austria
[b] Department of Biotechnology, Institute of Bioprocess Science and Engineering, University of Natural Resources and Life Sciences, Muthgasse 18, Vienna 1190, Austria
[c] Department of Material Science and Process Engineering, University of Natural Resources and Life Sciences, Peter-Jordan Strasse 82, Vienna 1190, Austria
[d] CICS-UBI–Health Sciences Research Centre, University of Beira Interior, Av. Infante D. Henrique, Covilhã 6201-506, Portugal
[e] Department of Chemistry, University of Beira Interior, R. Marquês d'Ávila e Bolama, Covilhã 6201-001, Portugal
[f] Department of Theoretical Chemistry, University of Vienna, Vienna, Austria
[g] Bioinformatics and Computational Biology, Faculty of Computer Science, University of Vienna, Vienna, Austria

ARTICLE INFO

Keywords:
IgG
Adsorption
Immunoglobulin
Small angle X-ray scattering
Affinity chromatography
Ligand density

ABSTRACT

Staphylococcal protein-A affinity chromatography has been optimized for antibody purification, achieving a current capacity of up to 90 mg/ml in packed bed. The morphology of the particles, the number of antibodies bound per ligand and the spatial arrangement of the ligands were assessed by *in-situ* Small-angle X-ray scattering (SAXS) and scanning electron microscopy (SEM) combined with measurement of adsorption isotherms. We employed SAXS measurements to probe the nanoscale structure of the chromatographic resin. From scanning electron microcopy, the morphology and area of the beads were obtained.

The adsorption isotherm revealed a bi-Langmuirian behavior where the association constant varied with the critical bulk concentration, indicating multilayer adsorption. Determining the antibody-ligand stoichiometry was crucial for understanding the adsorption mechanism, which was estimated to be 4 at lower concentrations and 4.5 at higher concentrations, suggestive of reversible protein-protein interactions. The same results were reached from the *in-situ* small angle X-ray scattering measurements. A stoichiometry of 6 cannot be achieved since the two protein A monomers are anchored to the stationary phase and thus sterically hindered.

Normalization through ellipsoids facilitated SAXS analysis, enabling the determination of distances between ligands and antibody-ligand complexes. Density fluctuations were examined by subtracting the elliptical fit, providing insights into ligand density distribution. The dense ligand packing of TOYOPEARL® AF-rProtein A HC was confirmed, making further increases in ligand density impractical. Additionally, SAXS analysis revealed structural rearrangements of the antibody-ligand complex with increasing antibody surface load, suggesting reversible association of antibodies.

1. Introduction

Staphylococcal protein A affinity chromatography is the crucial step for antibody purification and enables platform production processes [1,2]. Over the past decades, the ligand-structure has been improved, ligand density has been increased, and immobilization methods, bead porosity, bead size, and backbone have been refined to increase dynamic binding capacity and operational performance [3–8]. Dynamic binding capacity (DBC) of protein A media has been significantly improved, primarily by increasing the equilibrium binding capacity through the arrangement of repetitive antibody binding domains as one single ligand [9,10] and by increasing the number of binding domains [11,12].

However, despite the numerous efforts in industry and academia to improve this affinity chromatography material, there is still limited insight into the distribution of ligands available during the chromatographic process. The average ligand density does not reflect the spatial distribution of how far the different protein A ligands are apart and if the ligands are homogeneously distributed over the surface or crowed and

* Corresponding author at: Department of Biotechnology, Institute of Bioprocess Science and Engineering, University of Natural Resources and Life Sciences, Muthgasse 18, Vienna 1190, Austria.
E-mail address: alois.jungbauer@boku.ac.at (A. Jungbauer).

https://doi.org/10.1016/j.chroma.2024.465102
Received 16 April 2024; Received in revised form 14 June 2024; Accepted 16 June 2024
Available online 21 June 2024

leaving other areas blank. It has been questioned if all antibody binding domains in a protein A-ligand can be occupied. Ghose et al. [13] showed that in a tetrameric ligand, only 2.5 antibodies could bind on average. This has been corroborated with Protein A-coupled silica surrogate [14]. The non-stoichiometric ratio could be explained either by steric hindrance of the ligands or unequal distribution of the ligand. We demonstrated that the existence of heterogeneous binding sites and steric hindrance most probably causes the non-stoichiometric ratio of antibody - Protein A ligand formation [15]. Heterogenous binding site models can better fit the entire breakthrough curves [16] and microcalorimetric studies show results consistent with heterogeneous adsorption [17]. It seems that there is a preferred site that is occupied first at a 1:1 stoichiometry [18]. At high loadings, the antibody molecules can bind to the tetrameric ligand at a stoichiometry of 2:1. When the protein A column is overloaded, is difficult the interaction of a third antibody molecule due to steric effects, but we cannot exclude antibody self-interaction at these high concentrations. A multilayer formation has been observed at high loading [19].

The synthetic polymer-based protein A chromatography material AF-rProtein A HC-650F from Tosoh Bioscience exceeded for the first time at binding capacity over 80 mg/ml [20]. A mutated Staphylococcus aureus Protein A C domain has been immobilized in a hexameric form on Toyopearls HC 650 F [12]. The backbone is based on polyacrylates, one of the most popular types of resins for industrial applications. It has a particle porosity of ε_p= 0.5–0.8 and its rigid structure grants them greater mechanical strength, under typical operating conditions it form a non-compressible bed. This type of polymer-based chromatography media is produced by phase inversion, and the porous structure is formed by small polymer globules that stick together. Though, compared to agarose-based chromatography there exists no models for this type of synthetic chromatography materials.

In this work, we elucidated the binding orientation of the antibody-staphylococcal protein A complex through adsorption isotherms, SEM and SAXS analyses. The spatial ligand distribution, orientation, and stoichiometry of protein A to the resin TOYOPEARL ® AF-rProtein A HC is clarified. Before we established the model for the ligand and ligand distribution, we derived a model of the beads surface and depiction where the ligands could be potentially located. The beads' internal surface structure was visualized by SEM and to represent the substructure a spherical geometry was used. To follow the interaction between antibodies and the resin, TOYOPEARL ® AF-rProtein A HC was packed into a small column, and an *in-situ* monitoring of the loading, washing and elution chromatographic steps were made using SAXS as probing method. Results were complemented with adsorption isotherms.

2. Material and methods

2.1. Adsorption isotherms

A purified recombinant antibody (adalimumab, 144.2 KDa) was expressed in CHO and purified using Protein A chromatography. The antibody solutions were prepared in 0.02 M phosphate buffer with 0.15 M sodium chloride at pH 7.4 in a range from 0.01 to 10 mg/ml (Fig. 1a). A volume of 0.025 ml of resin was added to the antibody solution with a total volume of 0.25 ml. The samples were incubated for 24 h in a thermomixer (Thermo Fisher Scientific, Waltham, MA) at 20 °C and 900 rpm. After incubation, the bulk concentration was measured at wavelength of 280 nm using a UV plate reader (Tecan, Männedorf, Switzerland).

2.2. In-situ SAXS measurement

SAXS is a powerful and effective technique for determining molecule shapes and sizes at the nanoscale length and can also be applied to proteins when bound to a solid surface [21,22]. This approach measures the scattering intensity $I(Q)$ function of a scattering vector Q resulting from a scattering angle 2θ, at a given wavelength λ, where $Q = \frac{4\pi sin\theta}{\lambda}$. The SAXS measurements were performed at the Austrian beam line, Elettra, in Trieste, Italy.

After the incubation of the adsorption isotherms, the solution was resuspended, and 100 µL of incubated sample was loaded into a quartz capillary. The capillary was then placed aligned to the beam. The scattering images were collected during the whole chromatography run, with 1 s exposure for 370 frames using a 2D detector (Pilatus 1 M) at a photon energy of 8 keV. After this holding time, the system was equilibrated with 5 CV of running buffer, followed by 20 CV of glycine 0.1 M pH 3.5 for elution and a final 20 CV running buffer step for re-equilibration (Fig. 1b (2)-(4)).

For all SAXS measurements, spectra of the resin in elution buffer were subtracted from spectra in equilibration buffer (with and without protein). From the resulting spectra, pair density distributions (PDDS) were determined as described in the theory section below.

2.3. Scanning electron microscopy

The TOYOPEARL® AF-rProtein A HC beads were submerged in a cryoprotectant, 2.3 M sucrose solutions. The sample was then frozen with liquid nitrogen and the beads were cut into 30-µm thick slices using a tungsten carbide knife in an MT-990 Motorized Precision Microtome (RMC Boeckeler). The bead slices were dehydrated with ethanol series and then dried with CO_2 in a Critical Point Dryer Leica EM CPD030. For

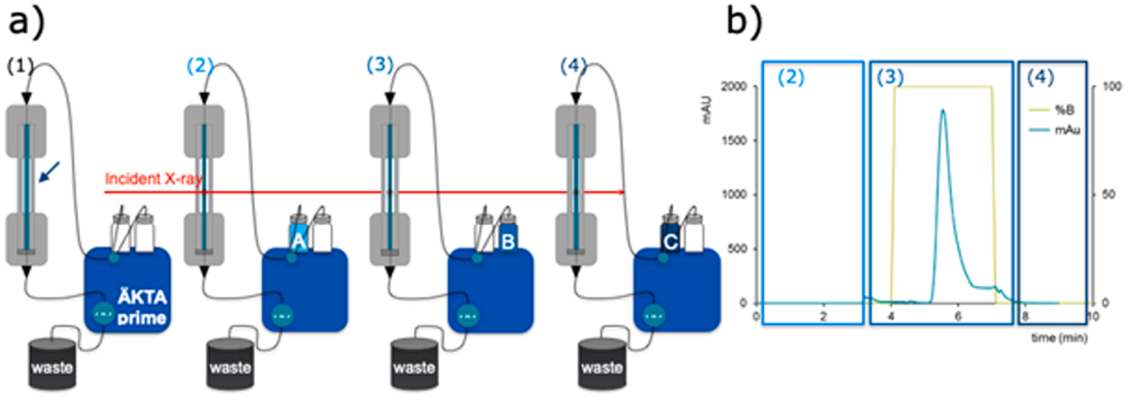

Fig. 1. a) The saturated resins were filled in a sample chamber (blue arrow) and settled under flow. The sample chamber was connected to an Äkta prime. b) The Äkta prime was operated remotely, and (2) wash (3) elution and (4) equilibration steps were conducted. Simultaneously, in these three steps, the resin was exposed to the X-ray beam, and scattering data were collected.

the visualization, we used a Scanning Electron Microscope Quanta™ 250 FEG, and the dried slices were placed on an aluminum slab and coated with a gold layer.

3. Theory

3.1. Pair densities from ellipsoids

The antibody binds to staphylococcal protein A ligands that are immobilized to a chromatography bead, which we consider as a fractal structure. This complex can be described by characteristic pair density distributions. In this work we chose the pair density distribution of an ellipsoid. We define the Fourier transform of the pair density distribution first. Then the Fourier transform of the pair density distribution is compared to the experimental scattering intensity, $I(Q)$.

$$P(R|Q) = \mathscr{F}(p(r|R))[Q] = \int_0^\infty p(r) J_{1/2}(Qr) \Big/ (Qr)^{1/2} \tag{1}$$

where $J_{1/2}$ is a Bessel function of the first kind of order ½. Next, we introduce the pair density distribution of a full sphere:

$$p_s^1(r|R) = \frac{3r^2(r-2R)^2(4R+r)}{16R^6} \tag{2}$$

R, resembles the radius of the sphere and r, the relative distances of the potential scattering sites therein. The pair density distribution is normalized to 1:

$$\int_0^{2R} dr p_s^1(r) = 1 \tag{3}$$

Following, we expand the pair density distribution of a sphere to an ellipsoid, we introduce a scaling function, $f(\lambda, x) = \sqrt{\lambda^2 x^2 - x^2 + 1}$, wherein $\lambda = a/b$, which is ratio of the two-half axis of the oblate ellipsoid. Note that in the present publication we chose $\lambda < 1$. For the oblate ellipsoid we compute the pair density distribution as follow:

$$p_{e,o}^1(r|a,b) = \int_0^1 dx\, H(2Rf(\lambda,x) - l) p_s^1(l/f(\lambda,x), R) \Big/ f(\lambda,x) \tag{4}$$

In fact, the radial density distribution, $\rho(r)$ of the oblate ellipsoid can be computed, too. It is given by:

$$\rho(r) = \frac{u^2}{a^2} \begin{cases} \sqrt{\frac{a^2}{b^2} - 1} & u < b \\ \sqrt{\frac{a^2}{u^2} - 1} & b \le u < a \\ 0 & 1 \end{cases} \tag{5}$$

The latter will be used for normalization.

3.2. Adsorption isotherm

The bi-Langmuir isotherm is the simplest model to account for surface binding heterogeneity, assuming the existence of high and low energy sites. This is how the equation appears:

$$q = \sum_{i=1}^{2} \frac{q_{i,m} K_i C}{1 + K_i C} \tag{6}$$

In Eq. (6) the association constant K_i is independent of the bulk concentration, C. We have made a simple phenomenological adaptation to this equation; we have changed the association constants concentration dependence (see Supplementary Information (Eq. S1-S7)). After introducing a critical bulk concentration, C_x, at which a second binding site becomes relevant, the bi-Langmuir can be read as follows:

$$\Gamma = \sum_{i=1}^{2} \frac{q_{m,i} K_i(C, C_x) C}{(1 + K_i(C, C_x) C)} \tag{7}$$

4. Results & discussion

4.1. Non-Langmuir adsorption behavior

The adsorption isotherm of the antibody binding to TOYOPEARL® AF-rProtein A HC is shown is Fig. 2 and can be fitted to a bi-Langmuir-based model using Eq. (7). The association constant changes according to the critical bulk concentration. This reflects the idea, that as of a certain bulk concentration the protein adsorbs as multilayer or the antibody-staphylococcus Protein A ligand complex rearranges, opening additional binding sites. However, macroscopic observations from the adsorption isotherm alone does not allow to conclude whether an antibody or the ligand itself serves as a binding site.

Another parameter that may allow us to understand whether protein-protein interactions or ligand rearrangements are causing bi-Langmuirian behavior is the antibody-ligand stoichiometry. This can be simply calculated via the number of ligands per ml bed volume (Eq. S15) and the binding capacity. The supplementary section provides an in-depth analysis of ligand density (Section 3 at the supplementary information). The resin network is reconstructed using 60 nm spheres arranged similarly to a pearl necklace (Section 2 at the supplementary information). Through this calculation, it was determined that each sphere accommodates approximately 55 protein A ligands (see supplementary material Eq. S16), resulting in a ligand distribution of 4.9×10^{-3} Lig. / nm^2 (Eq. S17). To reinforce our methodology, an alternative approach involving intra and extra-particle porosity was employed (Section 4 at the supplementary information), producing results closely resembling those previously obtained using the surface area of a 60 nm sphere. Based on this rational, at C_x (84 mg/ml), antibody ligand stoichiometry is estimated to be approximately equal to 4. At a stoichiometry of 4, four antibody molecules are binding to one hexameric ligand. Since the ligand is attached via multiple points, we hypothesize that ligand zones close to the attachment point sterically hinder the attachment of antibodies. One could envision the attachment of the ligand anchored at the two ends, allowing adsorption of the antibody onto the four central Protein A domains. This would be in line with previous reports [13] where a stoichiometry of 2.5 was determined for a tetrameric ligand.

At q_{max} of 95 mg/ml, antibody-ligand stoichiometry increases by 0.5 points. A stoichiometry of 4.5 could either indicate that energetically unfavored domains (close to the anchors) are populated at higher

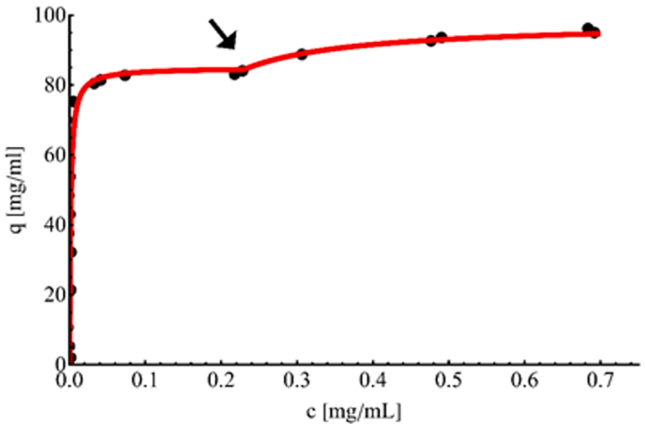

Fig. 2. Isotherm of the antibody adsorption to TOYOPEARL® AF-rProtein A HC. Note the kink in the isotherm. Full line, fit based on bi-Langmuir isotherm. Arrow indicates the critical bulk concentration, C_x.

concentrations or that higher protein concentrations induce reversible self-association, a common phenomenon in antibody solution studies [23].

Judging from the adsorption isotherm and antibody ligand-stoichiometry alone, we cannot favor either of both hypotheses. For a better understanding of the topology of the antibody, the resin, and their interactions, we opted for SAXS measurements.

4.2. The backbone a chain of ellipsoids?

In a chromatography bead the ligands are anchored at the backbone, which has a particular fractal form, and this results in a particular roughness, and thickness. In a recent work, we investigated the backbone structure of MabSelect SuRe, an agarose-based protein A media [15,18]. The morphology of TOYOPEARL® AF-rProtein A HC is different and thus we needed to adapt the recent approach that we termed pearl neckless model to fit scattering data of TOYOPEARL® AF-rProtein A HC.

When using SAXS for such intricate systems, data normalization is not trivial [15]. The structure of the analyzed objects should be known for fitting adequate models to the pair density distributions. In case of chromatographic resins, SEM offers a viable technique for the structural analysis. As shown in the SEM image given in Fig. 3a), TOYOPEARL® AF-rProtein A HC is a methacrylate polymer that assembles in rigid clusters. It consists of rigid particles where the solid density is very high. Microscopic magnification (Fig. 3b) show that the methacrylate polymer is organized as patches that are clustered to form the pore walls. With magnification, complete details were enlarged, and the resin borders were identified and colored yellow. It can be identified small white, blob-like patches that ellipsoids best could represent. Note that this boundary depends on the threshold by which pores are distinguished from resin and it appears that a narrower choice of walls could have been made. To overcome this limitation, we created an image that is binarized Fig. 3c). White areas represent resin, while dark gray areas are thought to be pores. We inserted exemplarily red ellipses in Fig. 3c, a binarized version of Fig. 3b, to bolster the analogy.

In line with our previous study [15] we analyzed the fractal dimension of the image and computationally generated the structure factor of the fractal network (Fig. S1 at the supplementary information), verifying a good match with an ellipsoidal shape.

4.3. TOYOPEARL® matrix consists of rigid polymethacrylate clusters

Another point of SAXS data normalization is related to background subtraction, considerations of how to preform it can be found at the supplementary material (Fig. S2) where is highlighted the complexity of

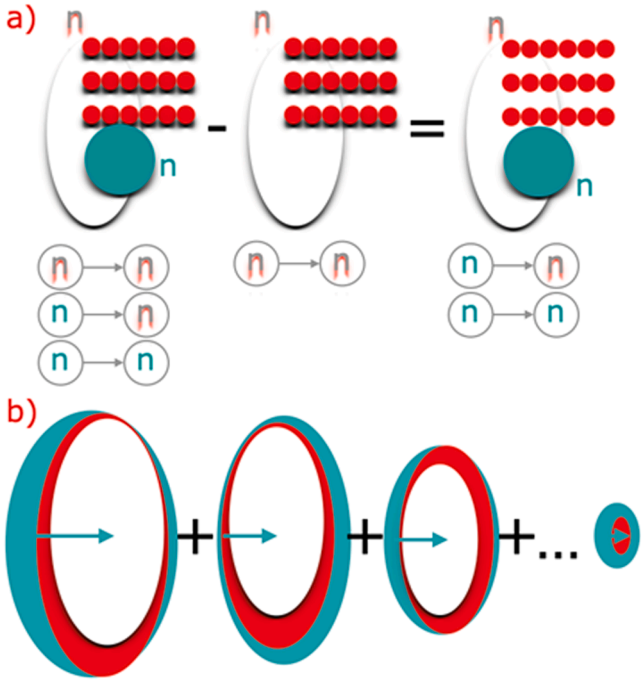

Fig. 4. a) Water-water, Water-resin, and water-protein interactions and conformational changes of the Protein-A ligand are neglected. Then if the pair density distributions (PDDS) from loaded resins were subtracted from PDDS of bare resins, the resulting PDDS is built from pairs in the protein (n, magenta) and pairs of the protein with the resin (n-magenta and n-gray with red shadow) b) The resin was filled with different sized ellipsoids, then SAXS accesses an average overall these differently sized objects.

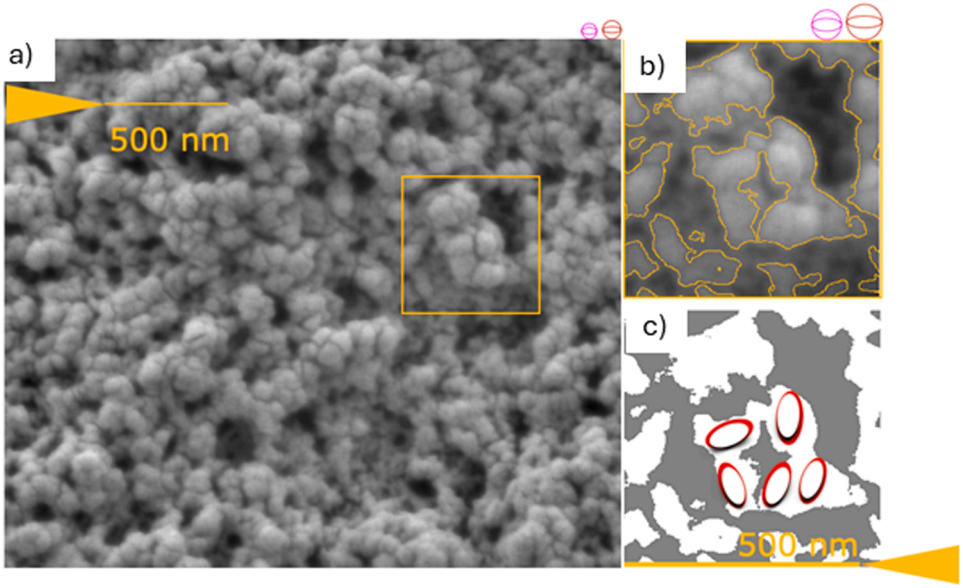

Fig. 3. a) Scanning Electron Microscopy (SEM) measurements taken from TOYOPEARL® AF-rProtein. b) A 500 nm complete detail of the SEM image; yellow borders indicate resin boundaries. c) The image was binarized: white areas indicate resin while gray areas indicate pores. The binarized image is exemplarily partly filled by ellipsoids. It is formed by a white core that reflects the resin, a red hull that reflects the protein-A ligand. If decorated by antibodies, the ellipsoid is covered by a cyan hull, which then demonstrates the antibody.

relating the scattering intensity to the pair density distribution. In Fig. 4a, we illustrate the challenge of normalizing the pair density distributions. Note that we have neglected water-water, water-resin, water-protein interactions, and conformational changes of the Protein-A ligand. Even so, despite subtracting background and resin pair distances, distances between the antibody and resin remain, which necessitates consideration when assessing density fluctuations. Moreover, when modeling the entire system, the total number of scattering sites is unknown. While we are aware of the number of the Protein-A ligand segments and the number of amino acids in the protein (represented by the cyan-colored n), we lack information on the total number proteins, ligands, and resin backbone scattering sites. We must assume that ligands surface density is homogeneous, as is the case for proteins in a loaded resin. In such instances, we do know that their pair density distribution is fractal and obey a power law. We propose that all scattering data comprises a summation of all different-sized ellipsoids, represented in Fig. 4. On average, it adds to a full ellipsoid comprising resin, Protein-A ligand, and antibody scattering sites.

Until this point, we have been mainly exploring the backbone of the stationary phase rather than delving into the specifics of the Protein A ligand. These ligands are immobilized on the resin backbone, with synthetically engineered Y domains from the native SpA C domains (PDB: 4ZMD) measuring 4.6 nm in length and 2.3 nm in width [24]. We provided a comprehensive model in a recent publication [15]. The net length of the ligand can be estimated; if stretched, it spans 27.6 nm. Employing Flory's theory, the ligand's end-to-end distance can be calculated using $R_F = \sqrt{N}l$, suggesting an average end-to-end distance of 11 nm, when anchored at two sites. We can envision the ligands being fractally distributed across the surface, forming fractal loops. By knowing the number of ligands per area, a distance of 15 nm can be

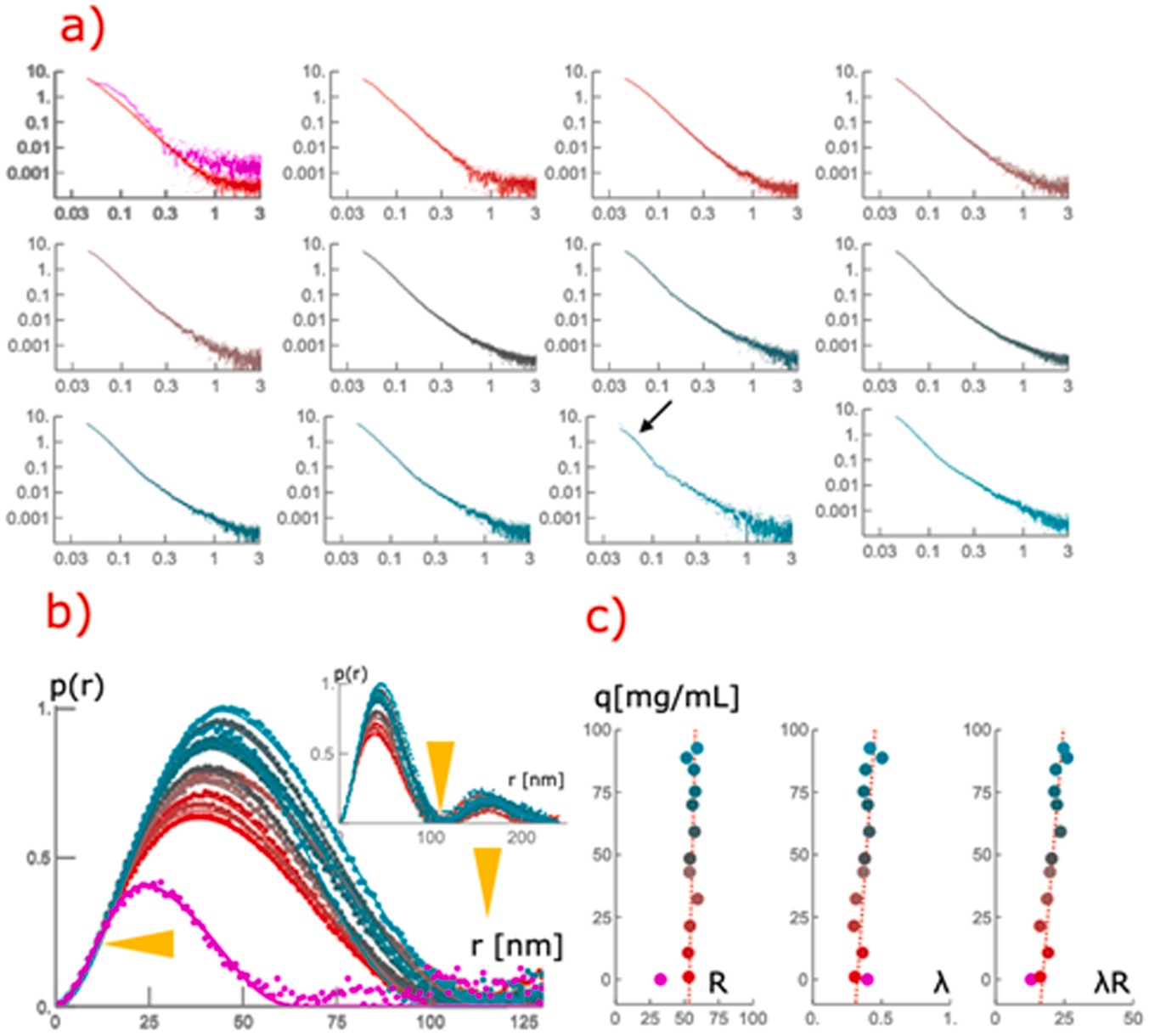

Fig. 5. a) Background subtracted individual points plot scattering intensities. Magenta points give background-subtracted scattering intensity of bare resin. Points colored red to cyan give background-corrected scattering intensities with increasing antibody surface load. Full lines in corresponding colors give fits to the experimental data. b) Pair density distributions were computed numerically (points) and then fitted by oblate ellipsoid pair density distributions. The maximum scale of the ellipsoid increases with increasing antibody surface load. c) Radius and aspect ratio (λ) of the elliptical fit. Actual antibody load of the data set can be read from the plot.

simply derived, assuming a simple hexagonal grid.

In summary, we have a model of the chromatographic resin and the immobilized ligands through SEM analysis, along with basic parameters such as ligand density and surface area. This framework greatly facilitates the subsequent SAXS analysis.

4.4. Scattering intensity profiles and elliptical fits

SAXS measurements recorded the scattering intensity profiles of antibody binding to TOYOPEARL® AF-rProtein A HC at different concentrations. The measurements were collected every second, and the structural changes at the different Q-range are shown through the scattering intensity plot in Fig. 5. The presence and respective antibody concentration change the scattering profile both in the low and high Q-range.

In Fig. 5 the background-subtracted scattering intensity of all 12 samples were given. The magenta-colored data points and lines indicate the scattering intensity of bare resin and their numerical fit. The average thickness of such blob-like patches is 66 nm in diameter which confirms the SEM results Fig. 3c). Complement background-corrected scattering intensities are color-coded. Red resembles a resin with minor amounts of antibody bound, while the intensity becomes more cyan colored as the amount of bound protein increases. Dots represent all experimental scattering data, while full lines depict fits to this data. Additionally, the color-coded dots in Fig. 5b correspond to the respective PDDS. Regarding the PDDS, we focused on the first peak and cut the PDDS at the right vertical yellow arrow. A second smaller peak was given in the insert in Fig. 5b. We normalize the PDDS and align them for pair distances shorter than 10 nm (left horizontal yellow arrow) for visualization purposes. This normalization is arbitrary.

The ellipsoidal shape indicated by SEM proved to be a valuable starting point for modeling the PDDS, as ellipsoidal PDDS closely matched the experimental data. The parameters of these ellipsoids are presented in Fig. 5. Interestingly, already small amounts of bound antibody change the best fit of the PDD. Without any bound protein, the radius was smaller (30 nm compared to 50 nm), with a higher sigma indicating a more spherical shape. This suggests that the antibody first binds to the apical regions, elongating the PDDS into a more ellipsoid shape. While the long half axis does not increase significantly, the smaller half axis does. It seems that initially ellipsoidal items become spherical again as antibodies load the resin, which indicates full occupation of the resin surface.

4.5. The radial density distribution a route to normalization?

The geometrical interpretation, while inspired by the SEM image, remains inherently arbitrary even though we have employed it for normalization. Its PDDS can interpret any ellipsoid, and thereof, we can compute the corresponding PDDS. An ellipsoid inherently has a center of reference, simplifying addition off PDDS as illustrated in Fig. 6. This approach offers the advantage that, under the assumption that no protein enters the resin, their local density should remain constant irrespective of the number of antibodies on top. This rationale aligns with arguments put forth in our previous work [15], justifying the alignment of the parabolic shapes in Fig. 6d).

In Fig. 6b), the PDDS illustrate the film growth process. The magenta line gave the PDDS of the bare resin, red the PDD of resins with small amounts of antibodies, and cyan with twice as many antibodies bound. By subtracting the magenta colored PDDS, we corrected the PDDS, with the results presented in Fig. 6c. Their net areas were plotted in Fig. 6d.

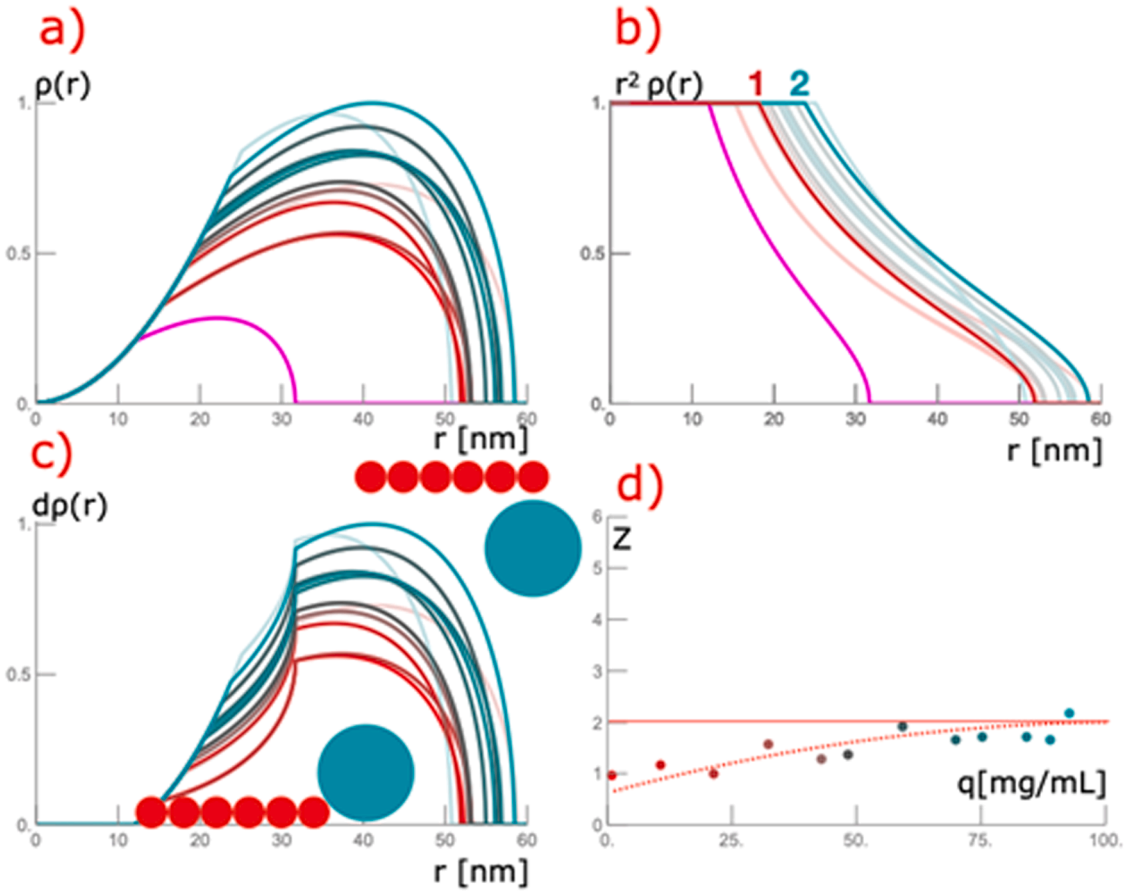

Fig. 6. a, b) Radial density distribution computed from PDDS. Radial density distribution was normalized concerning the parabolic shape for small r. c) Background corrected radial density distribution. d) The net area of the radial density distribution is proportional to the number of immobilizing proteins.

Normalizing the graph at $Q = 0$ revealed that the area occupied by antibodies doubles at higher concentrations compared to lower concentrations. The increase in net area of the radial distribution function correlates with loading of the resin. However, electron density of the antibody differs and therefore the increase of the area is only two-fold (unlike the 4-fold increase in antibody mass) at stoichiometry of 4. Furthermore, the maximum size of the ellipsoid increases by 7 nm from 52 nm to 59 nm which is close to the radius of hydration of an antibody of 5 nm [25]. That indicates saturation of the surface via monolayer adsorption without antibody-antibody interaction. Note that even at a stoichiometry of 4.5 under the assumption of protein-protein interactions, monolayer adsorption might still be possible via protein-protein interactions parallel to the surface.

At this point, our comprehension of the resin appears to be well-established. We have successfully linked real space data (SEM) to reciprocal space data (SAXS). Following the route of interpreting both data sets by ellipsoids, we can estimate film thickness and argue for the amount of bound antibody. While film growth provide insight into the average surface occupancy, it doesnt offer a detailed understanding of the nanoscale structure. For nanoscale understanding of the chromatographic resin, we determined density fluctuations by normalization with the elliptical fit.

4.6. Accessing density fluctuations by subtracting the elliptical fit

The elliptical fit offers another normalization route, where the elliptical fit of the PDD is subtracted from the PDD after transformation of the SAXS spectrum. The differences are the density fluctuations of the PDD. Explanation of how to find density fluctuations can be find on the supplementary material (Fig. 3S).

In Fig. 7, we give an estimate of the ligand density distribution of the investigated resin. For the resin without protein, maxima are found at 13, 30 and 60 nm. As we changed the SAXS evaluation, we come up with a similar but more phenomenological explanation.

As previously outlined, prominent distances are the average end-to-end distance of the hexameric ligand (11 nm) the distance between two ligands (15 nm) and the distance between next neighbors (30 and 60 nm). Those characteristic distances are maxima in the density fluctuations of the bare resin, as indicated in Fig. 7. It must be noted that the distances for the average end-to-end distance and the distance between the ligands are quite similar so they might be lumped together in the first maximum of the PDD (13 nm). The other maxima (30 and 60 nm) retrieved from the density fluctuations describe our considerations from macroscopic parameters extraordinarily well. With an average end-to-end distance between the two anchor points of the hexameric ligand of 11 nm and an average distance of 15 nm between neighboring ligands, the surface of TOYOPEARL® AF-rProtein A HC is densely packed. It appears unrealistic to further increase ligand density of the stationary phase, considering that the maximum dimension of an antibody is similarly large (D_{max} of 15–16 nm [25]). One could speculate about higher ligand density and thus higher binding capacities of a stationary phase carrying different ligands. For example, if a hexameric ligand with only one anchor point would be immobilized, binding capacities could increase. However, a surface with a high density of hexameric ligands could lead to diminished mass transfer effects, as antibodies would bind to the Protein A ligand that is the furthest away from the resin and sterically hinder other antibodies from reaching unoccupied Protein A segments. Consequently, the mass transfer of antibodies would be hindered, and antibodies could potentially not reach Protein A ligands closer to the resin surface.

In Fig. 8, we plotted the differences of analytical and numerical PDDS as function of increasing antibody surface load. The subtraction was done in such a manner that these density fluctuations are not computed negatively. We identified three peaks. Compared to the bare resin, the

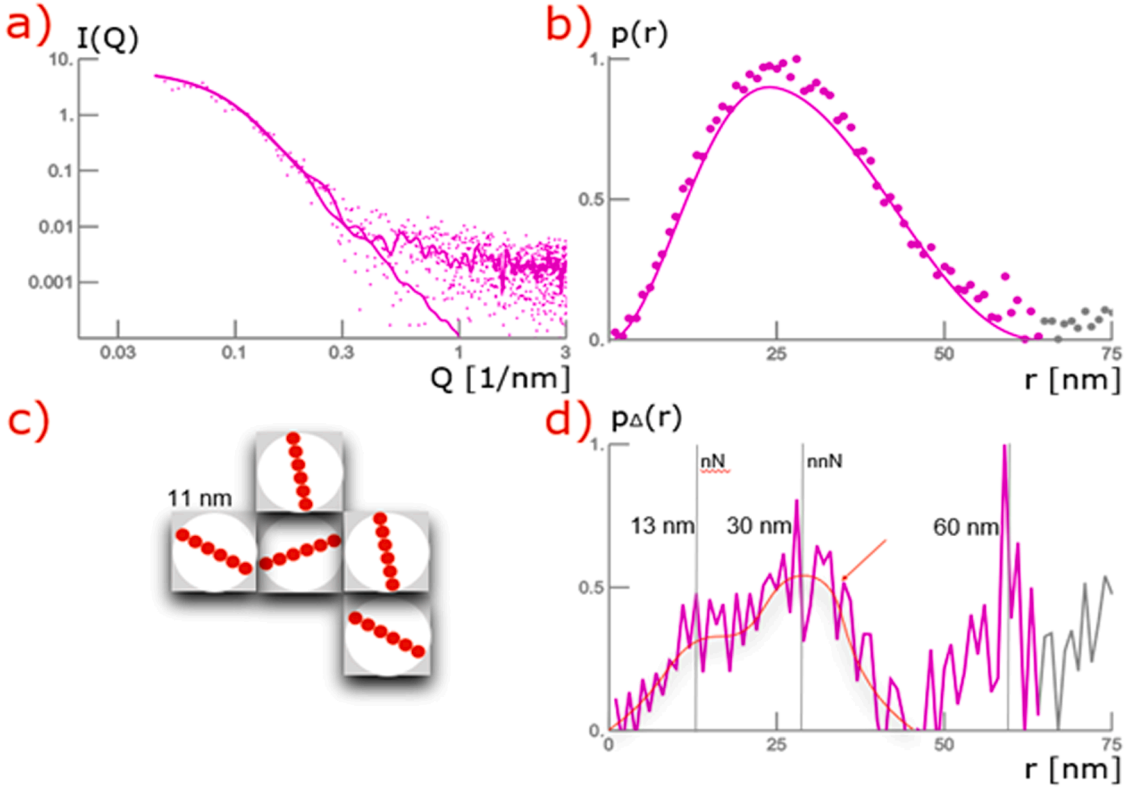

Fig. 7. a) Magenta points give background-corrected scattering intensity, I(Q) of bare resin. Full magenta lines correspond to pair densities computed numerically (fit) and calculated from PDDS from the ellipsoidal fit (b). b) Magenta points give pair densities calculated from the numerical fit, and full line indicate ellipsoidal fit of the pair density. c) A schematic fractal arrangement of Protein-A ligands d) The difference of both pair densities given in (b) result more than PDDS with a maximum at 13, 30, and 60 nm.

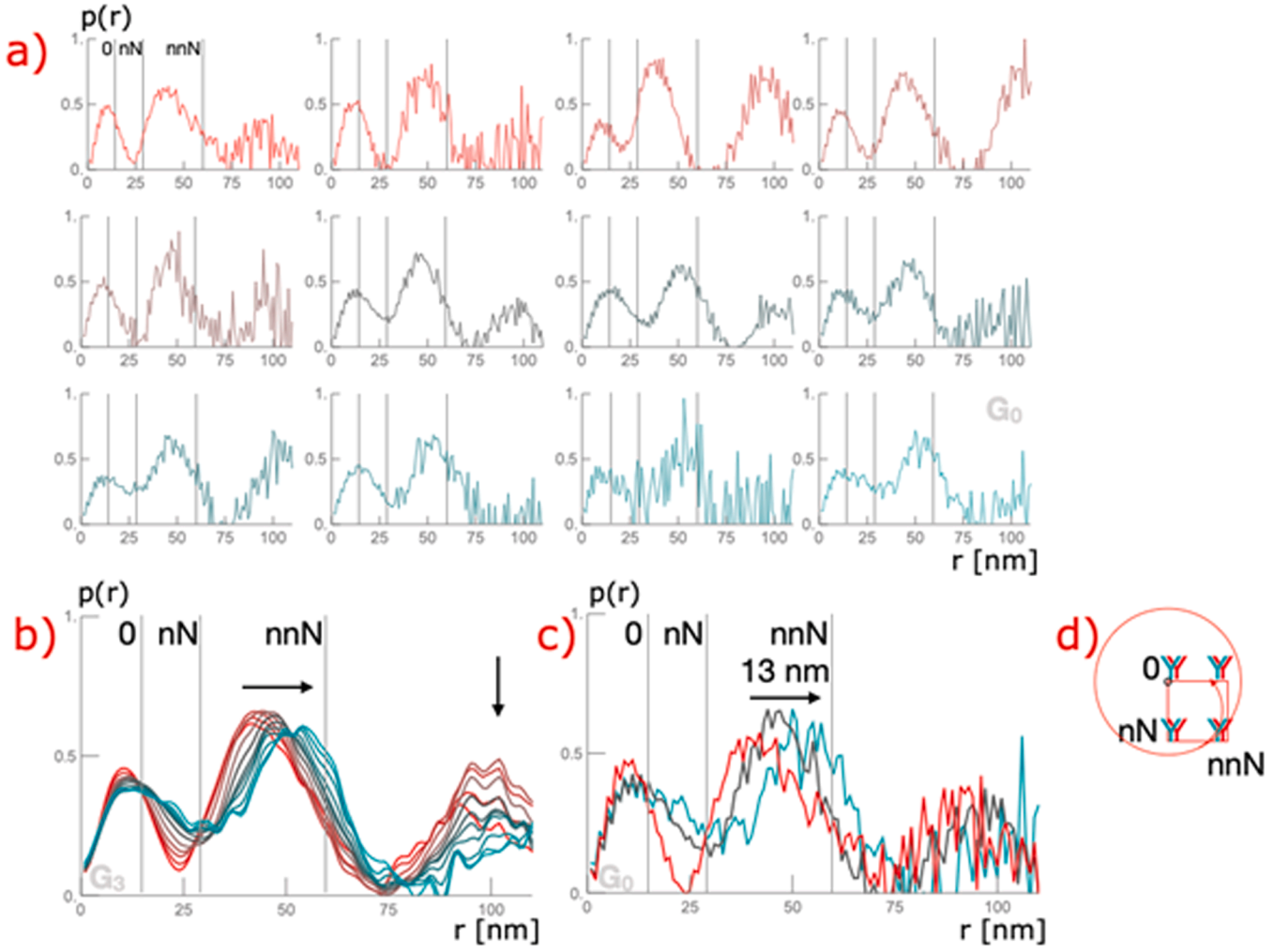

Fig. 8. a) Differences in pair densities, numerical and computed from ellipsoid fits, are given. Note the change of shape of the first and the second peak. b) Overly of the Gaussian filtered data. The first and the second peak shift to larger values indicating the filling to the Protein-A brush.

peak maxima are shifter towards larger distances. This indicates rearrangements of the antibody-ligand complex, potentially maximizing distances between the neighboring complexes. The smaller one can be assigned to the antibody-ligand complex. The bigger one can be attributed to the contributions of the next neighbors to the PDDS. The peak shapes changed with increasing antibody load and the valley between the peaks diminishes, indicating saturation of the surface. With growing load, the ligands are binding more than one antibody - the shoulder of the first peak increases. As mentioned, the second peak (increasing from 43 to 51 nm) can be attributed to the next neighbors. With higher antibody load, the distance between the neighbors increase from 43 nm to 51 nm could be explained by neighboring antibody-ligand complexes that orient in order to maximize their distances. This can only occur assuming nonuniform ligand-ligand distribution which is a reasonable assumption.

As seen in Fig. 8b, three highest antibody loads are above the critical antibody concentration, leading to higher binding capacities expected from conventional Langmuir behavior. Their corresponding PDDS display a splitting peak with a maximum at 51 and 56 nm, whereas PDDS with a lower mobile phase concentration show peaks below 51 nm. The distance between those peaks is 5 nm and therefore equal to the radius of gyration of an antibody [25]. As the stoichiometry also increases to 4.5, the second peak might arise due to an additional antibody binding to already bound antibodies. Ultimately, this suggests reversible association of an antibody to an already bound antibody. In the alternative scenario, in which the antibody binds to an unoccupied ligand, we would expect binding to one of the anchor points. In that case, correlation distances would not increase since the anchors are randomly distributed.

5. Conclusion

We have elucidated the binding orientation of the antibody-staphylococcal protein A complex through adsorption isotherms, SEM and SAXS analyses. We conclude that at the first plateau of the adsorption isotherm, monolayer adsorption with a stoichiometry of 4 occurs, suggesting that the hexameric ligand remains unoccupied at its two anchors. At the second plateau, the binding stoichiometry is 4.5 due to reversible protein-protein interactions. SAXS analysis corroborates these findings by revealing reversible protein-protein interactions, as evidenced by the increased distance between protein-antibody ligands. Both SEM images and SAXS Pair Density Distribution Functions (PDDS) suggests that the resin resembles an ellipsoidal structure. The normalization through ellipsoids allows normalization in SAXS, thereby allowing the determination of distances between ligands and the antibody-ligand complexes. The determined distance of 13 nm closely aligns with the calculated value of 15 nm assuming a hexagonal grid. However, the distance of the two anchor points cannot be determined via SAXS due to the similarity to the distance between the ligands, underscoring the close ligand packing of TOYOPEARL ® AF-rProtein A HC.

Funding information

Austrian Research Promotion Agency FFG – grant number 824186.

Portuguese Foundation for Science and Technology – CICS-UBI base grant with DOI 10.54499/UIDB/00709/2020 and CICS-UBI programmatic grant with DOI 10.54499 /UIDP/00709/2020.

CRediT authorship contribution statement

Rupert Tscheliessnig: Writing – original draft, Software, Investigation, Formal analysis. **Goncalo L. Silva:** Writing – original draft, Methodology, Investigation, Formal analysis, Data curation. **Jacek Plewka:** Methodology, Investigation, Formal analysis, Data curation. **Leo A. Jakob:** Methodology, Investigation, Formal analysis, Data curation. **Helga Lichtenegger:** Supervision, Formal analysis, Data curation, Conceptualization. **Alois Jungbauer:** Writing – review & editing, Supervision, Funding acquisition, Conceptualization. **Ana C. Dias-Cabral:** Writing – review & editing, Validation, Supervision, Methodology, Data curation, Conceptualization.

Declaration of competing interest

The authors declare that they have no known competing financial interests or personal relationships that could have appeared to influence the work reported in this paper.

Data availability

Data will be made available on request.

Acknowledgement

This work was supported by the Federal Ministry for Digital and Economic Affairs, the Federal Ministry for Transport, Innovation and Technology, the Styrian Business Promotion Agency SFG, the Standortagentur Tirol, Government of Lower Austria, and ZIT - Technology Agency of the City of Vienna through the COMET-Funding Program managed by the Austrian Research Promotion Agency FFG. And within the scope of the CICS-UBI base grant with DOI 10.54499/UIDB/00709/2020 (https://doi.org/10.54499/UIDB/00709/2020) and the CICS-UBI programmatic grant with DOI 10.54499 /UIDP/00709/2020 (https://doi.org/10.54499/UIDP/00709/2020) with national funds registered in the budget of the Foundation for Science and Technology. The funding agencies had no influence on the conduct of this research.

R.T. also received funding from Novo Nordisk Foundation grants NNF19OC0057834 and NNF21OC0066551.

Supplementary materials

Supplementary material associated with this article can be found, in the online version, at doi:10.1016/j.chroma.2024.465102.

References

[1] A.A. Shukla, B. Hubbard, T. Tressel, S. Guhan, D. Low, Downstream processing of monoclonal antibodies-application of platform approaches, J. Chromatogr. B Anal. Technol. Biomed. Life Sci. 848 (1) (2007) 28–39, https://doi.org/10.1016/j.jchromb.2006.09.026.

[2] A.A. Shukla, J. Thömmes, Recent advances in large-scale production of monoclonal antibodies and related proteins, Trends Biotechnol. 28 (5) (2010) 253–261, https://doi.org/10.1016/j.tibtech.2010.02.001.

[3] R. Hahn, P. Bauerhansl, K. Shimahara, C. Wizniewski, A. Tscheliessnig, A. Jungbauer, Comparison of protein A affinity sorbents: II. Mass transfer properties, J. Chromatogr. A 1093 (1–2) (2005) 98–110, https://doi.org/10.1016/j.chroma.2005.07.050.

[4] R. Hahn, R. Schlegel, A. Jungbauer, Comparison of protein A affinity sorbents, J. Chromatogr. B Anal. Technol. Biomed. Life Sci. 790 (1–2) (2003) 35–51, https://doi.org/10.1016/S1570-0232(03)00092-8.

[5] R. Hahn, K. Shimahara, F. Steindl, A. Jungbauer, Comparison of protein a affinity sorbents III. Life time study, J. Chromatogr. A 1102 (1–2) (2006) 224–231, https://doi.org/10.1016/j.chroma.2005.10.083.

[6] A. Jungbauer, R. Hahn, Engineering protein A affinity chromatography, Curr. Opin. Drug Discov. Dev. 7 (2) (2004) 248–256.

[7] M. Linhult, S. Gülich, T. Gräslund, A. Simon, M. Karlsson, A. Sjöberg, K. Nord, S. Hober, Improving the tolerance of a protein a analogue to repeated alkaline exposures using a bypass mutagenesis approach, Proteins Struct. Funct. Genet. 55 (2) (2004) 407–416, https://doi.org/10.1002/prot.10616.

[8] T.M. Pabst, J. Thai, A.K. Hunter, Evaluation of recent Protein A stationary phase innovations for capture of biotherapeutics, J. Chromatogr. A 1554 (2018) 45–60, https://doi.org/10.1016/j.chroma.2018.03.060.

[9] V. Amritkar, S. Adat, V. Tejwani, A. Rathore, R. Bhambure, Engineering Staphylococcal Protein A for high-throughput affinity purification of monoclonal antibodies, Biotechnol. Adv. 44 (2020), https://doi.org/10.1016/j.biotechadv.2020.107632.

[10] J. Scheffel, S. Hober, Highly selective protein A resin allows for mild sodium chloride-mediated elution of antibodies, J. Chromatogr. A 1637 (2021), https://doi.org/10.1016/j.chroma.2020.461843.

[11] M. Freiherr von Roman, S. Berensmeier, Improving the binding capacities of protein A chromatographic materials by means of ligand polymerization, J. Chromatogr. A 1347 (2014) 80–86, https://doi.org/10.1016/j.chroma.2014.04.063.

[12] E. Müller, J. Vajda, Routes to improve binding capacities of affinity resins demonstrated for Protein A chromatography, J. Chromatogr. B Anal. Technol. Biomed. Life Sci. 1021 (2016) 159–168, https://doi.org/10.1016/j.jchromb.2016.01.036.

[13] S. Ghose, B. Hubbard, S.M. Cramer, Binding capacity differences for antibodies and Fc-fusion proteins on protein A chromatographic materials, Biotechnol. Bioeng. 96 (4) (2007) 768–779, https://doi.org/10.1002/bit.21044.

[14] A.R. Mazzer, L.A. Clifton, T. Perevozchikova, P.D. Butler, C.J. Roberts, D. G. Bracewell, Neutron reflectivity measurement of protein A–antibody complex at the solid-liquid interface, J. Chromatogr. A 1499 (2017) 118–131, https://doi.org/10.1016/j.chroma.2017.03.084.

[15] G.L. Silva, J. Plewka, H. Lichtenegger, A.C. Dias-Cabral, A. Jungbauer, R. Tscheliessnig, The pearl necklace model in protein A chromatography: molecular mechanisms at the resin interface, Biotechnol. Bioeng. 116 (1) (2019) 76–86, https://doi.org/10.1002/bit.26843.

[16] E.X. Perez-Almodovar, G. Carta, IgG adsorption on a new protein A adsorbent based on macroporous hydrophilic polymers. I. Adsorption equilibrium and kinetics, J. Chromatogr. A 1216 (47) (2009) 8339–8347, https://doi.org/10.1016/j.chroma.2009.09.017.

[17] G.F.L. da Silva, J. Plewka, R. Tscheliessnig, H. Lichtenegger, A. Jungbauer, A.C. M. Dias-Cabral, Antibody binding heterogeneity of protein A resins, Biotechnol. J. 14 (8) (2019) e1800632, https://doi.org/10.1002/biot.201800632.

[18] J. Plewka, G.L. Silva, R. Tscheließnig, H. Rennhofer, C. Dias-Cabral, A. Jungbauer, H.C. Lichtenegger, Antibody adsorption in protein-A affinity chromatography – *in situ* measurement of nanoscale structure by small-angle X-ray scattering, J. Sep. Sci. 41 (22) (2018) 4122–4132, https://doi.org/10.1002/jssc.201800776.

[19] K. Behere, S. Yoon, n-Layer BET adsorption isotherm modeling for multimeric Protein A ligand and its lifetime determination, J. Chromatogr. B Anal. Technol. Biomed. Life Sci. 1162 (2021), https://doi.org/10.1016/j.jchromb.2020.122434.

[20] W. Krepper, P. Satzer, B.M. Beyer, A. Jungbauer, Temperature dependence of antibody adsorption in protein A affinity chromatography, J. Chromatogr. A 1551 (2018) 59–68, https://doi.org/10.1016/j.chroma.2018.03.059.

[21] A.Z. Komaromy, C. Kulsing, R.I. Boysen, M.T.W. Hearn, Salts employed in hydrophobic interaction chromatography can change protein structure - insights from protein-ligand interaction thermodynamics, circular dichroism spectroscopy and small angle X-ray scattering, Biotechnol. J. 10 (3) (2015) 417–426, https://doi.org/10.1002/biot.201400465.

[22] C. Kulsing, A.Z. Komaromy, R.I. Boysen, M.T.W. Hearn, On-line determination by small angle X-ray scattering of the shape of hen egg white lysozyme immediately following elution from a hydrophobic interaction chromatography column, Analyst 141 (20) (2016) 5810–5814, https://doi.org/10.1039/c6an00851h.

[23] B.J. Dear, J.A. Bollinger, A. Chowdhury, J.J. Hung, L.R. Wilks, C.A. Karouta, K. Ramachandran, T.Y. Shay, M.P. Nieto, A. Sharma, J.K. Cheung, D. Nykypanchuk, P.D. Godfrin, K.P. Johnston, T.M. Truskett, X-ray scattering and coarse-grained simulations for clustering and interactions of monoclonal antibodies at high concentrations, J. Phys. Chem. B 123 (25) (2019) 5274–5290, https://doi.org/10.1021/acs.jpcb.9b04478.

[24] M. Salvalaglio, L. Zamolo, V. Busini, D. Moscatelli, C. Cavallotti, Molecular modeling of Protein A affinity chromatography, J. Chromatogr. A 1216 (50) (2009) 8678–8686, https://doi.org/10.1016/j.chroma.2009.04.035.

[25] A. Narvekar, S.L. Gawali, P.A. Hassan, R. Jain, P. Dandekar, pH dependent aggregation and conformation changes of rituximab using SAXS and its comparison with the standard regulatory approach of biophysical characterization, Int. J. Biol. Macromol. 164 (2020) 3084–3097, https://doi.org/10.1016/j.ijbiomac.2020.08.148.